Journal of Marine Research, 41, 427–460, 1983

On the mean dynamical balances of the Gulf Stream Recirculation Zone

by James C. McWilliams[1]

ABSTRACT

The time mean circulation is analyzed at a site on the southern edge of the Gulf Stream Recirculation Zone (31N, 70W) from data taken in the POLYMODE Local Dynamics Experiment. Additional mean quantities are described from a combination of dynamical assertions and inferences. The mean vorticity balance is examined to infer the mean vertical velocity and eddy relative vorticity flux divergence. The vertical velocity is found to be mostly upward and an order of magnitude larger than the downward surface Ekman pumping. In the mean heat, salt, density, and potential vorticity budgets, the mean advections of these quantities are nonzero, and substantial eddy flux divergences are again required for balance. These are inferred to be primarily associated with mesoscale eddies. The corresponding horizontal eddy diffusivities for these quantities are large ($\approx 10^8$ cm^2 s^{-1}) over an extensive depth range, from the surface to at least 4000 m. An assessment is also made of the likelihood of a homogeneous potential vorticity layer in the Recirculation Zone. From our estimates of the local potential vorticity gradients, there is no clearly indicated zero gradient layer, and the qualitative features of our local estimates are consistent with the larger-scale analysis of McDowell *et al.* (1983).

1. Introduction

The purpose of this paper is to describe the local time mean state of the ocean, commonly referred to as the general circulation, from data taken over several years at 31N, 70W, the site of the POLYMODE Local Dynamics Experiment (LDE).[2] Inferences of several aspects of the general circulation which were not directly measured will be made from the associated dynamical balance equations. The balances are assumed to be geostrophic and hydrostatic, time derivatives are neglected in the balance equations, and the time mean stretching vorticity is assumed dominant over mean relative vorticity. The first two assumptions are traditional and reliable. The last two are plausible from scale estimates. The upper surface boundary condition is an Ekman velocity, and the lower one is no flow normal to the sloping bottom. Several eddy flux divergences, associated with fluctuations in time about the mean state, are inferred to be significant. Among these are the horizontal eddy fluxes of heat, salt, momentum, and potential vorticity. Inferences of eddy flux divergences in mean

1. National Center for Atmospheric Research, Boulder, Colorado, 80307, U.S.A.
2. The LDE is described in McWilliams *et al.* (1982).

balance equations are of considerable interest because direct observations of eddy fluxes at the LDE site, and elsewhere, are too spatially limited at present to permit credible divergence calculations and to span the ocean depth. The directly measured fluxes from the LDE are, however, valuable as consistency checks upon the inferred flux divergences.

Diagnoses of the general circulation and its dynamical balances cannot be made explicitly and completely with current oceanographic observing techniques. Too many relevant quantities are inaccessible; e.g., mean vertical velocity and diapycnal diffusivity. Hence, the diagnoses must be inferential and significantly dependent upon the diagnostician's dynamical assumptions. Some recent examples of such diagnoses, each with its own particular assumptions, are Stommel and Schott (1977), Davis (1978), Wunsch (1978), and Keffer and Niiler (1982).

The present study is akin to those above. It is, however, based upon presumed knowledge of the vertical profiles of mean horizontal velocities, as well as profiles of the mean hydrographic quantities: temperature, salinity, and pressure. Most previous diagnoses have only presumed knowledge of the latter, and hence have had to infer the horizontal velocities, at least at one level, the reference level. The LDE site is one of the few in the world where velocity measurements of sufficient duration and vertical resolution have been made so that a diagnostic method can be based upon them. We shall find, however, that even in such a well-measured location as this, the sampling errors in determining the means are not comfortably small. That is, even if our dynamical assumptions are correct, some of the inferred properties of the general circulation are significantly uncertain. This is a general defect of extant ocean observations and diagnoses, and it must be accepted in our pursuit of the general circulation.

The LDE site is within the Gulf Stream Recirculation Zone, which is a northwestern intensification of the circulation within the interior of the North Atlantic Subtropical Gyre. This feature is shown schematically in Figure 1a, with the site also marked. Note that the site appears to be on the southern edge of the zone. The LDE velocity measurements confirm this (Section 2): the flow exhibits the Return Flow character (i.e., flow with a component to the west) in the thermocline but is reversed at greater depths. The mean wind stress in this location produces a downward Ekman velocity at the upper surface (Fig. 1b), which is characteristic of the Subtropical Gyre. The bottom topography is quite smooth, characteristic of the Hatteras abyssal plain, with a gentle slope up toward the Bermuda rise (Fig. 1c).

The contents of this paper are as follows. The directly measured mean horizontal velocities and hydrographic quantities are discussed in Section 2. Subsequently, inferences are made of mean vertical velocity and the eddy flux of relative vorticity (Section 3), eddy fluxes of heat, salt, and density (Sections 4 and 5), and mean potential vorticity gradients (Section 6). Some remarks about the mean energy and momentum balances are presented in Section 7, and Section 8 is a summary.

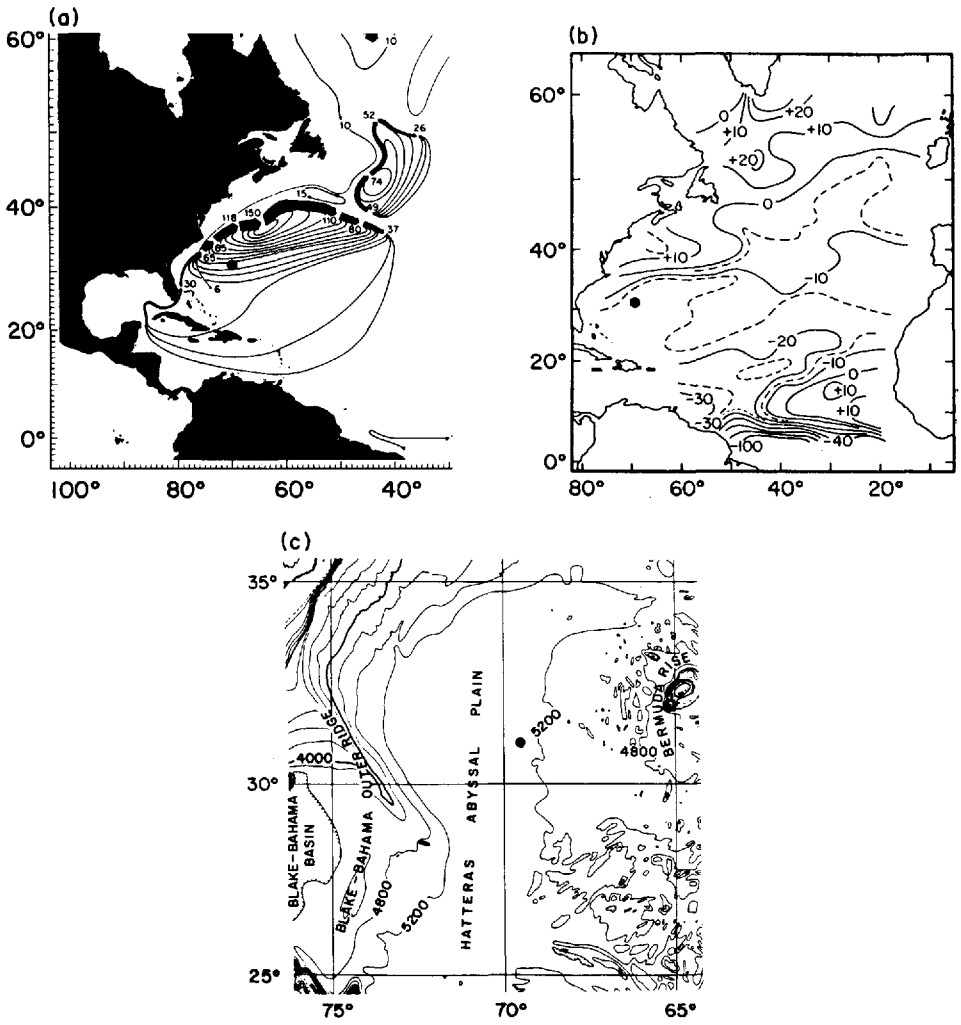

Figure 1. The large-scale environment of the Gulf Stream Recirculation Zone. The LDE site is marked with a dot. (a) A schematic of the depth integrated mean circulation in Sv, with a contour interval of 10 Sv (Worthington, 1976, Fig. 42); (b) the annual mean vertical velocity at the base of the Ekman layer, in units of 10^{-5} cm s^{-1} (Leetmaa and Bunker, 1978, Fig. 3); (c) depth contours in m (Uchupi, 1971).

2. Horizontal velocities and hydrographic quantities

The LDE data we shall base our analyses on are of two types: temperature T, salinity, S, and pressure, P, from hydrographic profiling instruments and east and north velocity, u and v, from moored current meters. The averaging and smoothing of each of these is discussed below.

a. Hydrographic quantities. In each of the three years 1977–1979, a set of hydrographic profiles was made, and for each set an average $T(P)$ and $S(P)$ has been calculated. In April 1977, a LDE site survey cruise was made (Bradley *et al.*, 1977; Ebbesmeyer *et al.*, 1983). The 1977 average is taken over the six profiles from that cruise which reached as deep as 5460 db, within 100 km of the LDE center. Subsequent manipulations of the data are made on a uniform P grid with spacing 20 db. In May–July 1978, seven hydrographic surveys were made on an array with spacing 25 km and radius 100 km (Taft *et al.*, 1983). The average T and S profiles span 0–3017.5 db with spacing 2.5 db. In July 1979, 10 profiles were taken within 50 km of the LDE center (Bryden and Millard, 1980). The average spans 0–5029 db with spacing 2 db.

The averaging among profiles within each data set is insufficient to eliminate small-scale structure in the profiles. Since this structure is implausibly present in the true mean, we shall smooth the profiles until a subjectively satisfactory degree of smoothness is achieved, with retained scales of 100 m and larger. We do this in stages. The more highly differentiated quantities discussed in later sections will require additional smoothing beyond that applied here. The smoothing will be accomplished by repeated applications of a Gaussian 3-point filter: for any quantity γ_i with a grid index i, the formula is

$$\gamma_i \leftarrow \frac{1}{4}\gamma_{i-1} + \frac{1}{2}\gamma_i + \frac{1}{4}\gamma_{i+1}, \tag{1}$$

with an endpoint formula of

$$\gamma_1 \leftarrow \frac{3}{4}\gamma_1 + \frac{1}{4}\gamma_2 \tag{2a}$$

or

$$\gamma_1 \leftarrow \frac{1}{2}\gamma_1 + \frac{1}{2}\gamma_2, \tag{2b}$$

with analogous formulae at the other endpoint. The alternatives (2a) and (2b) either tend to preserve the quantity value or diminish its derivative at the endpoint, respectively. For most quantities we shall apply (2a); (2b) will be applied only to horizontal velocities and Brunt-Väisälä frequency at the top or bottom of the ocean.

First we smooth the P profiles of S and T. The formulae (1) and (2a) are applied 10, 30, and 30 times, respectively, to each of the years' data sets (n.b., fewer applications are required to achieve a given degree of smoothness for a quantity on a grid with coarser spacing, in this case the 1977 data). The results are shown in Figure 2a, a plot of potential temperature θ against S. Note that the three data sets nearly coincide at depth (smaller θ and S values); more precisely, they agree to within 0.005 0/00 in S at a given θ below 3°C. Near the surface (above 18°C), they differ considerably due to

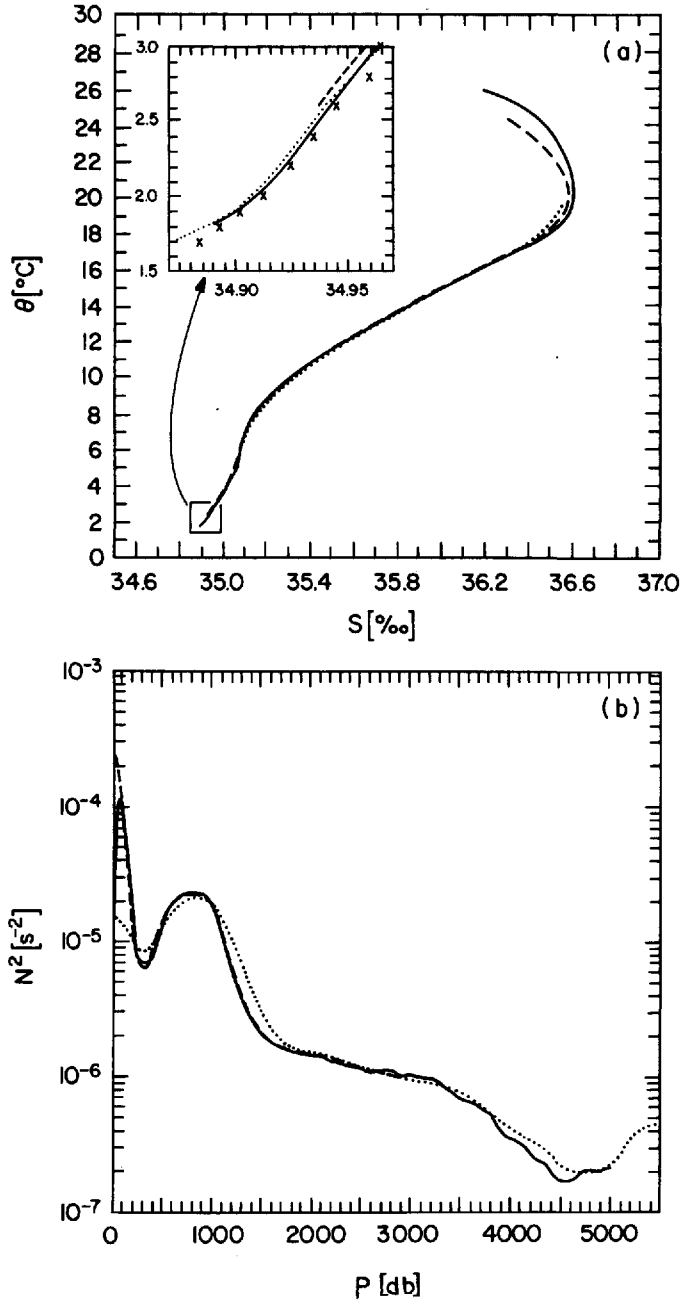

Figure 2. Mean quantities from the three hydrographic data sets: 1977, dotted line; 1978, dashed; 1979, solid. (a) Potential temperature (using the formula of Bryden, 1973) and salinity; (b) the square of the Brunt-Väisälä frequency N. Smoothing is as described in the text. The crosses in the insert in panel (a) are taken from the charts of Worthington and Wright (1970).

their differing phases in the seasonal cycle. Other locations of noticeable differences are the lower thermocline (7–11°C) and the Mediterranean water (4–6°C), although these differences are likely sampling errors associated with mesoscale variability [see Taft *et al.* (1983) for profiles of S variance]. The slight change in slope below 2°C is associated with Antarctic Bottom Water. It is of interest that here, and continuing in θ up to 3°C, all of our profiles are fresher, typically by about 0.005 0/00, than measurements taken during the late 1950s (Worthington and Wright, 1970). However, because of geographical interpolation uncertainties, titration errors (Fofonoff, 1963), standard water variations (Mantyla, 1980), and, possibly, mesoscale variations, we cannot be completely confident this difference is a true decadal scale change in the deep ocean, although it likely is because the estimated uncertainty from the various sources is not larger than the estimated signal. Additional evidence for decadal-scale freshening of deep water in the North Atlantic has been reported in TTO (1981).

Another display of the hydrographic data sets is the plot of mean Brunt-Väisälä frequency in Figure 2b. N^2 is here calculated from the three set-averaged T and S profiles over pressure intervals of 40, 5, and 16 db, respectively, and then smoothed using Eqs. (1) and (2) 30, 500, and 1000 times. In $N(P)$ the data set differences are larger than in $S(\theta)$, though still reasonably small. The local maximum near the surface, of differing strengths in the different profiles, is in the seasonal thermocline; the minimum near 300 db is in the 18°C thermostad; the broad peak near 750 db is in the main thermocline; and the small peak near the bottom is in the Antarctic Bottom Water. Some of the differences in Figure 2b are likely due to differing degrees of smoothing: for example, the weaker extrema for the thermostad and main thermocline in the more smoothed 1977 data.

We shall estimate mean hydrographic profiles as composites of the three data set averages shown in Figure 2. This is done as a linear combination; for a quantity γ_i, we calculate the mean as

$$\gamma_i = \sum_j \alpha_i^j \gamma_i^j \tag{3}$$

where the next j ranges over the data sets and i over pressure. The coefficients are defined as follows:

P [db]	α^{77}	α^{78}	α^{79}
i	i	i	i
0–2500	0	1	0
2500–3010	$(P-2500)/1020$	$(3010-P)/510$	$(P-2500)/1020$
3010–4500	½	0	½
4500–5020	½ + $(P-4500)/1040$	0	$(5020-P)/1040$
5020–5460	1	0	0

(4)

The 1978 data are given greatest weight where they are available, because of their

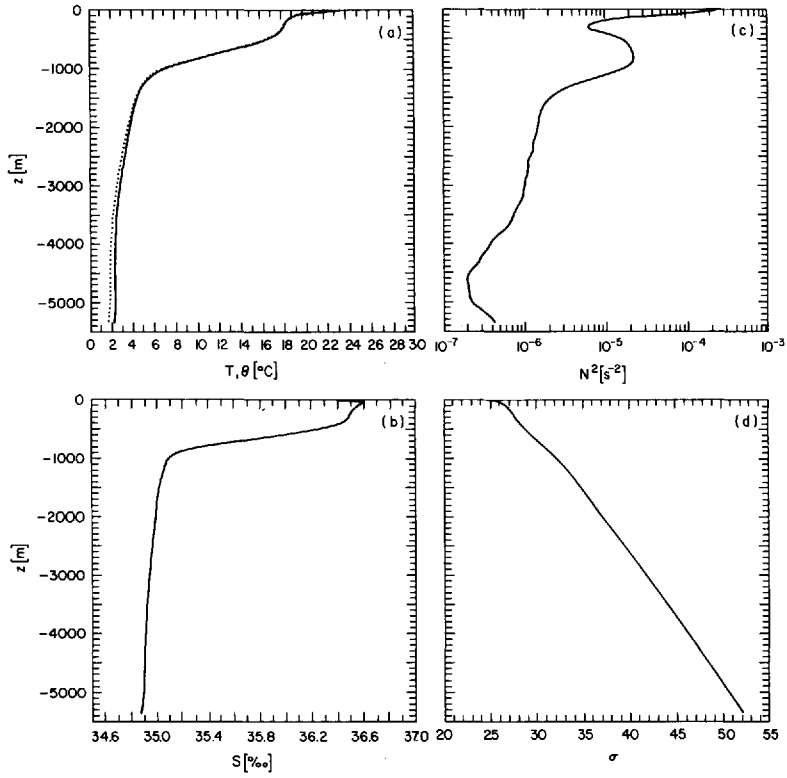

Figure 3. Depth profiles of mean hydrographic quantities: (a) T and θ (solid and dashed lines, respectively), (b) S, (c) N^2, (d) σ.

abundance, and the other two years are given equal weights. The formula (3) is applied to T, S, and N^2, and, from the first two of these, additional hydrographic quantities are calculated. Among these is density ρ. From density and the hydrostatic assumption, the depth is calculated as

$$z = -\int_0^P dP/g\rho, \tag{5}$$

where g is the gravitational constant. We now transform all pressure profiles to depth profiles. The results are shown in Figure 3: T, θ, S, N^2, and σ, where σ is the density anomaly,

$$\sigma = 10^3 (\rho - \rho_0) \tag{6}$$

and ρ_0 is a reference density of 1 gm cm^{-3}. The mean ocean depth is 5350 m, as determined by local soundings in the LDE. The curves in Figure 3 show the same hydrographic regimes identified in Figure 2: the two thermoclines, the 18°C thermostad, the deep water layer, and Antarctic Bottom Water. These features in the density

anomaly are, however, somewhat masked by the monotonic increase due to compressibility.

Obviously there is a degree of arbitrariness in the hydrographic data smoothing as just described. However, this arbitrariness is inconsequential for the qualitative character of the conclusions to be drawn below on vertical scales larger than about 100 m. Nor is the arbitrariness large compared to the sampling uncertainties in estimating the mean, as represented by the differences between the three profiles in Figures 2a and 2b.

b. Horizontal velocities. Horizontal velocities were measured at 10 depths at the LDE center for intervals of up to 15 months between May 1978 and July 1979 (Owens *et al.*, 1982). Two types of time averages are calculated at each depth, one over the full record interval, whatever its length, and the other over a particular, uniformly sampled, 290-day interval when all instruments were working. Both types of averages are plotted in Figure 4, together in panel (a) and separately in panels (b) and (c). The sampling errors in these averages are not small. They vary with velocity component and depth, but are approximately 2 cm s^{-1} in and above the main thermocline and 1 below (*ibid*).

A particular form of samping error, of potential concern, is due to the episodic nature of the LDE site velocities: three times during the years 1977–1979, an intense, southwestward, thermocline jet occurred, lasting for about a month (McWilliams *et al.*, 1982). Do such events seriously contaminate the mean velocity estimates? In my opinion, they do not. Owens *et al.* (1982, Fig. 4) computed mean velocities excluding the periods during which jets occurred and found qualitatively similar mean profiles to those in Figure 4, albiet with smaller amplitude. On the other hand, one must be cautious in interpreting a mean obtained from a sample containing a few distinctive events, in addition to general eddy variability, particularly when the mean has some structural similarity with the events.

Within the sampling uncertainties there is considerable scope for estimating the true LDE mean. In particular, we cannot refute the hypothesis that $u \equiv v$ at all z, which if true would have strong dynamical consequences (n.b., Sections 4–6). Because of these uncertainties, we shall work with several estimates of the mean, each of which is consistent with the sample averages, and only some of which assume $u \equiv v$. These alternatives do not span the full range of possibilities, but do expose the sensitivities of inferred quantities to the uncertainties. It is the uncertainties in the velocity profiles, rather than the hydrographic profiles, which most imperil our inferences. The uncertainty in velocity, as a fraction of the estimated mean, is much greater than that in potential temperature, for example.

The several estimates of the mean velocity profile are also plotted in Figure 4. They are subjective interpolations of the point measurements from current meters, selected by the principle of incorporating greatest smoothness in z, while closely fitting the data

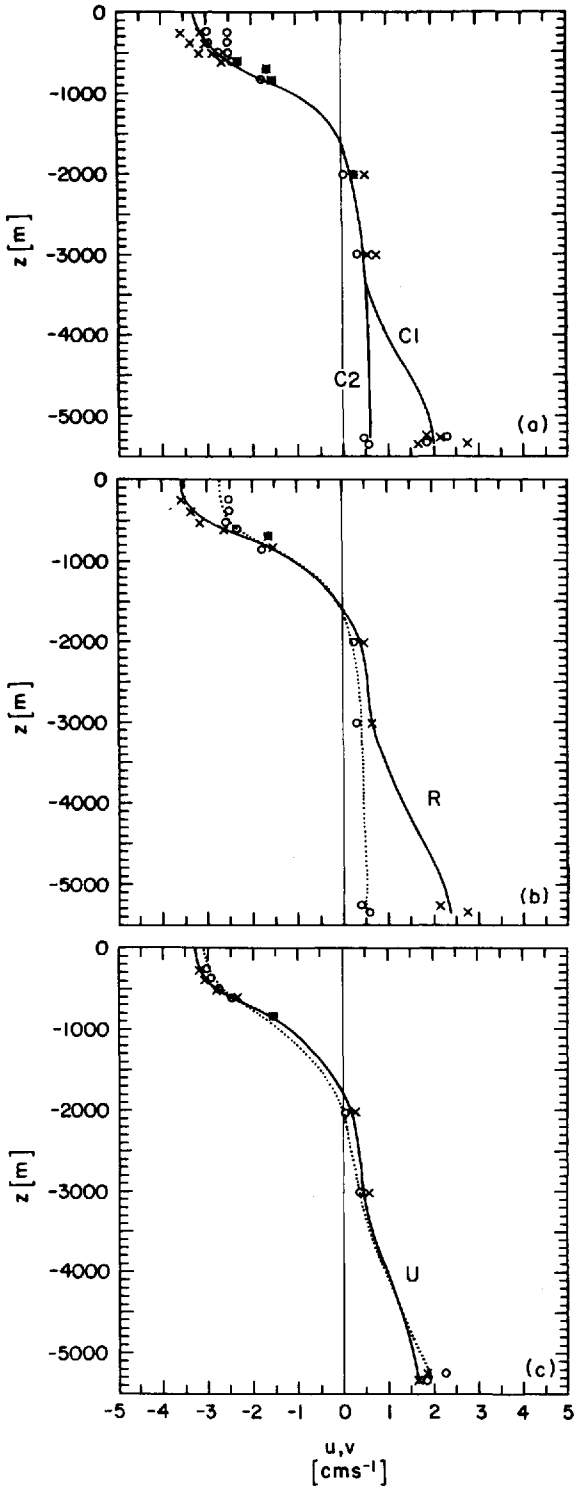

Figure 4. Mean horizontal velocity measurements (x = u; 0 = v) and interpolated depth profiles: (a) both types of averages and composite profiles C1 and C2, assuming $u = v$; (*b*) full record averages and profile R with $u \neq v$ (u is plotted as a solid line and v as a dotted line); (c) 290 day, uniformly sampled averages and profile U with $u \neq v$.

values. Those in panel (a) are constrained by the condition $u \equiv v$, and are fit to the composite data set, containing both components and both types of averages. Profile C1 includes a velocity enhancement near the bottom, as indicated by most of the data, while profile C2 has nearly uniform flow in the bottom 2 km, as indicated by the full-record-average v components near the bottom. In my opinion C2 is a less likely estimate of the mean than C1, although still within the sampling uncertainties. Panels (b) and (c) (profiles R and U) are for the two different types of averages, with the u and v data fit separately.

We shall now discuss these LDE velocity profiles in the context of other estimated mean velocities from moorings in the Recirculation Zone, as well an idealization of the Recirculation Zone mean circulation within and beneath the thermocline (Fig. 5). This idealization represents a spatially smooth conception of the general circulation and is consistent with the available long-term average velocities from current meters located in topographically smooth regions, as well as certain gross characteristics of numerical model solutions (see below). It is undoubtedly falsely simple in topographically rough regions (e.g., near Bermuda), and it certainly should not be given too much credence away from the indicated locations of available data.

The LDE velocity profiles show a Return Flow of several cm s^{-1} to the southwest in and above the thermocline. This is what we identify as the defining characteristic of the Recirculation Zone, as sketched in Figure 1a. This is also consistent with the direct current measurements of a zone of westward flow at 600 m depth extending for about 400 km to the south of the Gulf Stream along 55W (Schmitz, 1980); see Figure 5. The vertical shear above $z = -1800$ m in Figure 4 has the same shape as that calculated for this location from the historical archive of hydrographic profiles, but the historical magnitudes are only half as large (Lindstrom *et al.*, 1980); this discrepancy can be attributed to the large horizontal smoothing interval (400 km) in the historical analysis. The LDE site is distinct from the MODE site 300 km to its south, outside the Recirculation Zone, where the thermocline mean flow is small and probably eastward (Tarbell and Spencer, 1978).

Below the thermocline the flow is oppositely directed to the northeast, which we call the Reverse Flow (Fig. 5). Its magnitude is a fraction of a cm s^{-1} at 2000 and 3000 m depth and several cm s^{-1} near the bottom. The mean flow is similarly directed to the northeast at a site 200 km closer to the Gulf Stream (32°40′N, 70°50′W). There the magnitude is a fraction of a cm s^{-1} at 1100 m depth and several cm s^{-1} from 3250 m to the bottom (Pillsbury *et al.*, 1982). We therefore conclude that there is a reasonably large zone of deep mean flow opposite in sign to the thermocline Return Flow along 70W. This is also seen along 55W (Schmitz, 1980, and Fig. 5), although there the magnitude at 4000 m depth is only about 1 cm s^{-1}. Along 55W, this Reverse Flow zone is to the south of a band of deep Return Flow of relatively narrow width ($\approx$200 km). Presumably a deep Return Flow occurs across 70W as well, to the north of 33N, although this is as yet undocumented. In the deep water as well, the MODE site mean

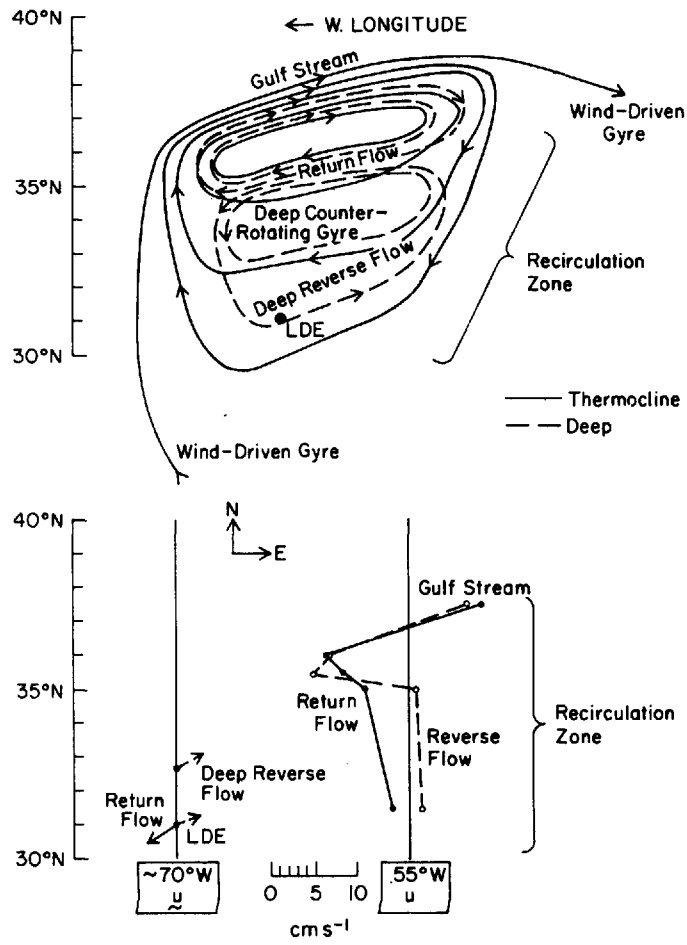

Figure 5. A schematic drawing of mean circulation at two levels for the northwest quadrant of the North Atlantic Subtropical Gyre (upper panel) and a depiction of observed mean velocities at two longitudes from sources discussed in the text (lower).

velocity (Schmitz, 1977) is much smaller (and oppositely directed) compared to the Reverse Flow at the LDE site and farther north.

Modeling results exhibit somewhat analogous features in the mean circulation. Often a pair of gyres occurs in the deep ocean, one corotating, one counterrotating, relative to a broader-scale thermocline Recirculation Gyre (Holland, 1978; Schmitz and Holland, 1982); this structure is also drawn in Figure 5. Across central meridians, this double gyre structure appears as a sequence of alternating currents: the Gulf Stream in the north, the Return Flow in the middle, and the Reverse Flow in the south.

c. Horizontal gradients. As a consequence of sampling errors, we cannot rely on direct estimates of horizontal gradients of mean hydrographic quantities and velocities, even though the LDE included arrays spanning either 200 km (hydrography) or 50 km (moorings). With only one exception, the estimated gradients are small compared to their standard errors, $l(2\sigma^2/N)^{1/2}$, where σ^2 is the variance of the quantity in question, l is the horizontal span of the measurements, and N is the number of independent samples; values for these quantities are reported in Owens *et al.* (1982) and Bryden (1982) for the mooring data. The one exception is the eastward derivative of northward velocity, $\partial v/\partial x$, whose estimated value (i.e., 5×10^{-7} s^{-1} at ~700 m depth; Bryden, 1982, Table 4) is at least not much smaller than its standard error, and which therefore has some credibility as to sign and order of magnitude. This estimate indicates a moderate southward turning of the thermocline Return Flow as it passes through the LDE site. This feature, if real, is too much of a local detail to be seen in the highly idealized Figure 5. For the LDE hydrographic data, the sampling errors are such that no significant horizontal gradients were resolved beneath the surface boundary layer: the 1977 and 1979 measurements are few in number and the two-month time interval in the 1978 data is too brief. The historical archive of all hydrographic data, as analyzed by Lindstrom *et al.* (1980), does show significant gradients (see Section 2b above), but only after smoothing over a very large spatial area. Perhaps a more local analysis of the archive, augmented by the LDE hydrographic data, would yield a sufficiently accurate estimate of horizontal gradients, but this has not been done, since in principle it is redundant with $\mathbf{u}(z)$ (see Section 4).

Thus, sampling limitations in the data preclude extensive use of direct estimates of local mean horizontal gradients and force us to rely on inferrential estimates, such as using the thermal wind relation (23) to estimate $\nabla\theta$ in Section 4.

3. Vertical velocity and vorticity

Vertical velocity cannot be measured directly, at least not with sufficient accuracy to obtain a credible mean. Hence it must be inferred. We shall do this from the mean vorticity equation (i.e., the vertical component of the curl of the momentum equations), which we write as

$$f\frac{\partial w}{\partial z} - \beta v - \nabla \cdot (\overline{\mathbf{u}'\zeta'}) = \mathbf{u} \cdot \nabla\zeta, \tag{7}$$

with neglected terms of higher order in Rossby number, as is usual in the quasigeostrophic approximation. In (7), w is the vertical velocity, f is the Coriolis frequency, β is its y derivative (i.e., northward), boldface denotes a horizontal vector, the prime denotes a fluctuation about the mean, the overbar denotes a time mean (n.b., for simplicity the overbar is deleted from most mean quantities; e.g., we write w instead of

$\overline{w}$), and ζ is the relative vorticity

$$\zeta = \frac{\partial v}{\partial x} - \frac{\partial u}{\partial y}. \tag{8}$$

The mean vorticity equation (7) has, by definition, no time derivative term, $\partial\zeta/\partial t$. However, our estimated means from the LDE cannot be distinguished in practice from very low frequency components. This does not prevent our neglecting $\partial\zeta/\partial t$, as can be seen by the following scale estimate. The ratio of the relative importance of $\partial\zeta/\partial t$ in (7) is

$$\frac{\partial\zeta}{\partial t}/\beta v \sim (L\tau\beta)^{-1},$$

where L and τ are respectively the horizontal and temporal scales for variations of the general circulation. From Figures 1a and 5, we can estimate L as a few hundred km (200 km, say). τ is even less well known, but by the absence of obvious trends in the LDE time series, it is at least as long as a year. Thus,

$$(L\tau\beta)^{-1} \lesssim [(2 \times 10^7 \text{ cm})(3 \times 10^7 \text{ s})(2 \times 10^{-13} \text{ cm}^{-1} \text{ s}^{-1})]^{-1} = 0.01,$$

which justifies our neglect of the tendency term. Even if we were to substitute for u/L the questionable, directly estimated ζ from Section 2c and (8), the preceding ratio would increase only to .05, still a small number. By a similar argument we can also neglect the mean advection of relative vorticity in (7); viz.,

$$\frac{\mathbf{u} \cdot \nabla\zeta}{\beta v} \sim \frac{u}{\beta L^2}$$

$$\approx \frac{(2 \text{ cm s}^{-1})}{(2 \times 10^{-13} \text{ cm}^{-1} \text{ s}^{-1})\,(2 \times 10^7 \text{ cm})^2} = 0.03,$$

which is small. This justifies the neglect of the final term in (7).

We therefore arrive at an equation for w:

$$w(z) = w_s(z) + \frac{1}{f}\int_z^0 dz' r(z'), \tag{9}$$

where w_s is the Sverdrup velocity,

$$w_s(z) = w_E - \frac{\beta}{f}\int_z^0 v(z')dz', \tag{10}$$

w_E is the mean Ekman velocity (-1.5×10^{-4} cm s^{-1} in the LDE region; Fig. 1b), and r is the eddy relative vorticity flux divergence,

$$r(z) = -\nabla \cdot (\overline{\mathbf{u}'\zeta'}). \tag{11}$$

The Sverdrup velocities (10) are shown in Figure 6 for the four different $\mathbf{u}$ profiles of Figure 4. They are negative near the top surface, as forced by the Ekman layer, but

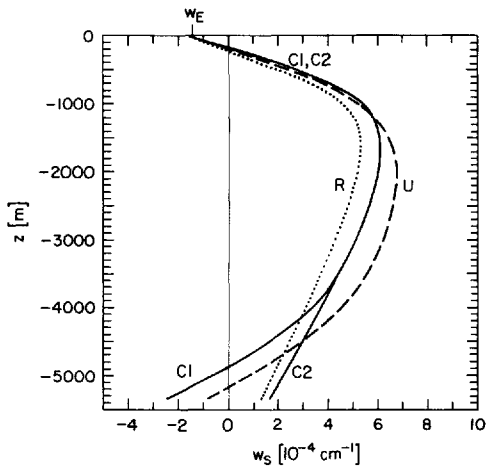

Figure 6. The Sverdrup component of mean vertical velocity from(10), with w_E and $\nu(z)$ taken from Figures 1b and 4, respectively. The labels correspond to those of the horizontal velocity profiles in Fig. 4: profiles C1 and C2 are drawn as solid lines, profile R as dotted, and profile U as dashed.

only in a small depth range. They are positive throughout most of the water column. The mid-depth values are large compared to w_E, and hence not very sensitive to it. The bottom values are scattered about zero: the average for the four profiles is -0.1×10^{-4} cm s^{-1}, which is indistinguishable from zero within sampling errors. This implies that the meridional transport here is equal to the Sverdrup transport, fw_E/β ($= -0.5 \times 10^5$ cm^2 s^{-1}). This result would be consistent with

$$r_0 = \frac{1}{H}\int_{-H}^{0} dz' r(z') \tag{12}$$

equal to zero in (9) and either a flat ocean bottom or zero horizontal velocity across topographic contours, so that $w = 0$ at the bottom. However, we can show that this is not the correct bottom condition.

The bottom boundary condition of no flow normal to the ocean bottom can be expressed as

$$w(-H) = \mathbf{u}(-H) \cdot \nabla \triangle H, \tag{13}$$

where the ocean bottom is the surface $z = -H + \triangle H(\mathbf{x})$. From the topographic chart (Fig. 1c), we see that the local bottom slope is about 10^{-3} up to the east, if we assume a horizontal averaging scale of 100 km or so. A more precise value (Pratt, 1968) is

$$\nabla(\triangle H) = (1.5, -0.3) \times 10^{-3}. \tag{14}$$

This is the same slope value used by Price and Rossby (1982) in demonstrating that topography has an important influence on deep mesoscale variability in the LDE.

Table 1 lists the consequent bottom velocities from (13) and (14) along with the

Table 1. Vorticity quantities.

$\mathbf{u}(z)$ Profile	$w(-H)$ $[10^{-4}\,\mathrm{cm\,s^{-1}}]$	$w_s(-H)$ $[10^{-4}\,\mathrm{cm\,s^{-1}}]$	r_o $[10^{-13}\,\mathrm{s^{-2}}]$
C1	24	−2.5	3
C2	7	1.6	1
R	34	1.3	4
U	20	−0.9	2

Sverdrup velocities (10) for comparison. $w(-H)$ is very much larger than $w_s(-H)$, and these two quantities cannot be made equal within our estimated uncertainties. Hence the eddy relative vorticity flux cannot be neglected. Its depth average, r_0, can be calculated from (9) evaluated at $z = -H$:

$$r_0 = f/H\,[w(-H) - w_s(-H)]. \tag{15}$$

Values for r_0 from (15) are also listed in Table 1.

These r_0 values can be compared with calculations of $\overline{\mathbf{u}'\zeta'}$ from LDE moored velocity measurements in the thermocline (unfortunately, there is insufficient horizontal resolution to calculate r directly). E. Brown and W. B. Owens (personal communication) obtain $|\overline{\mathbf{u}'\zeta'}| = 0.4 \times 10^{-5}\,\mathrm{cm\,s^{-2}}$. A scale estimate for r is therefore

$$|\overline{\mathbf{u}'\zeta'}|/L = 2 \times 10^{-13}\,\mathrm{s^{-2}},$$

using the same L of 200 km as before. This is quite similar to the inferred, depth-average values r_0 in Table 1. Calculations of the empirical, orthogonal functions for the vertical structure of mesoscale eddies in the LDE also indicate that the most energetic mesoscale variability is only weakly depth-dependent (Owens, 1983). Together these results suggest that $r(z)$ is also only weakly depth dependent. Consequently, we shall adopt a depth-independent model for it (i.e., $r(z) = r_0$). Hence, the inferential formula for total vertical velocity is

$$w(z) = w_s(z) - r_0 z/f. \tag{16}$$

These profiles are plotted in Figure 7. w is almost everywhere positive and tends to increase systematically with depth. Its magnitude is moderately sensitive to $\mathbf{u}(-H)$, as indicated, for example, by the much smaller w values for profile C2, which has a relatively small $\mathbf{u}(-H)$. If $r(z)$ were moderately surface intensified, which is the most likely sense in which $r \equiv r_0$ is too crude, then the profiles in Figure 7 would have the same end values but more outward bulge in between. Thus, the simple formula (16) is more likely to underestimate mid-depth w than overestimate it.

The magnitude of w_s is about $5 \times 10^{-4}\,\mathrm{cm\,s^{-1}}$ at the base of the thermocline, and the w value there is slightly larger due to $r(z)$. If these values were typical of the Recirculation Zone, whose area can be estimated at $2 \times 10^{16}\,\mathrm{cm^2}$ from Figure 1a, then an upward transport through the thermocline of about $10^{13}\,\mathrm{cm^3\,s^{-1}}$ would be occurring.

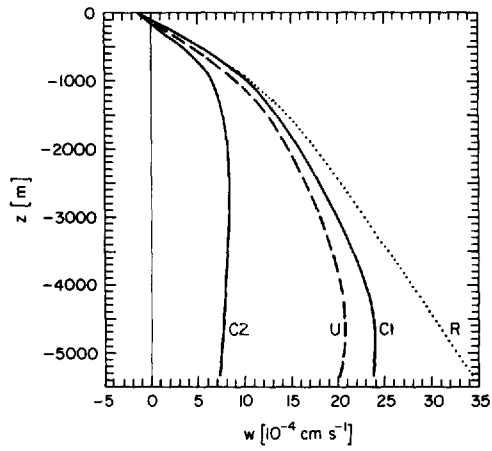

Figure 7. Total mean vertical velocity from (16). w_s is taken from Figure 6 and r_0 from Table 1.

This latter figure is comparable to present estimates of sub-polar water mass sinking rates (Worthington, 1976). We note, however that the large LDE w_s values result from a substantial southward v in and above the thermocline; this may not be characteristic of the whole Recirculation Zone, and thus the total upwelling could be much less than the above estimate. In addition, for the reason discussed in the next paragraph, we do not expect $r_0 > 0$ everywhere in the Recirculation Zone, which provides a further caution about estimating total vertical transport from the LDE. Accompanying the w in Figure 7 is a mean divergence of about 5×10^{-9} cm^{-1} s^{-1}, broadly distributed through the water column.

We can interpret r_0 crudely as an eddy diffusion process if we identify r with $\nu\nabla^2\zeta$, where ν is a horizontal eddy viscosity. The previously described estimate of $\zeta \approx \partial v/\partial x$ in the thermocline indicates it is positive at the LDE. If we further assume that the Recirculation Zone spatial structure is more oscillatory than exponentially growing or decaying—as does seem to be true for the flow patterns in the schematic Figure 5—then $\nabla^2\zeta$ will most often have the opposite sign of ζ. $r_0 > 0$ and $\nabla^2\zeta < 0$ imply $\nu < 0$; i.e., the relative vorticity flux would be counter-gradient. We shall return to this issue in Sections 6 and 7.

4. Heat

The mean heat balance equation in the interior can be written

$$\mathbf{u} \cdot \nabla\theta + w\frac{\partial\theta}{\partial z} = -\nabla \cdot (\overline{\mathbf{u}'\theta'}) - \frac{\partial}{\partial z}(\overline{w'\theta'}), \tag{17}$$

neglecting molecular conduction. This equation, as written, is not based upon a small Rossby number assumption.

From previous calculations, we know most of the quantities on the left side of (17); in particular, the vertical profiles of $\mathbf{u}$, w, and $\partial\theta/\partial z$. We can calculate the remaining quantity $\nabla\theta(z)$ from a thermal wind relation based upon geostrophic, hydrostatic, and Boussinesq approximations, yielding

$$-\boldsymbol{e}_z \times \frac{g}{f\rho_0} \nabla \rho = \frac{\partial \mathbf{u}}{\partial z}, \tag{18}$$

a linearization of the equal of state for sea water,

$$\delta\rho = -\rho_0[\alpha_T(z)\delta\theta + \alpha_S(z)\delta S], \tag{19}$$

and an assumption of local homogeneity of water masses, implying a strong correlation between θ and S variations,

$$\delta S = \mathcal{S}(z)\delta\theta. \tag{20}$$

In (18), $\boldsymbol{e}_z$ is a unit vertical vector. In (19), α_T and α_S are coefficients of thermal and saline expansion,

$$\alpha_T = -\frac{1}{\rho_0}\frac{\partial\rho}{\partial T}, \qquad \alpha_S = -\frac{1}{\rho_0}\frac{\partial\rho}{\partial S}, \tag{21}$$

evaluated at each z with the mean T, S, and P values. Compressibility effects are neglected (e.g., an α_P in (19), or the difference between an α_θ and an α_T). The prefix δ in (19) and (20) denotes any infinitesimal variation of the indicated quantity. The quantity $\mathcal{S}(z)$ in (20) is calculated as

$$\mathcal{S}(z) = \frac{dS(z)}{d\theta(z)}, \tag{22}$$

the derivative of the composite $S(\theta)$ constructed from Figure 2a. Combining (18)–(22), we obtain the desired expression for $\nabla\theta(z)$,

$$\nabla\theta = \frac{-f}{g[\alpha_T + \mathcal{S}\alpha_S]}\boldsymbol{e}_z \times \frac{\partial}{\partial z}\mathbf{u}. \tag{23}$$

Horizontal temperature advection can therefore be written as

$$\mathbf{u}\cdot\nabla\theta = \frac{f}{g[\alpha_T + \mathcal{S}\alpha_S]}\left(u\frac{\partial v}{\partial z} - v\frac{\partial u}{\partial z}\right). \tag{24}$$

A similar relation was derived by Bryden (1976). For the particular circumstance where $u(z) \equiv v(z)$, as in profiles C1 and C2 in Figure 4, this advection vanishes. Even in profiles R and U, where $u \not\equiv v$, there is a considerable tendency for cancellation in (24).

Thus, all quantities on the left side of (17) are known. Unfortunately, those on the

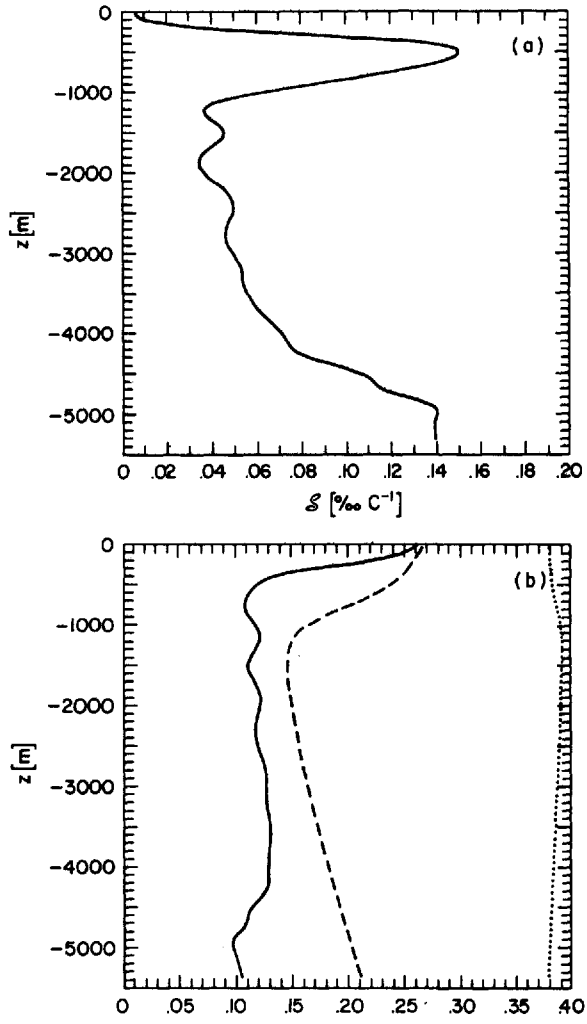

Figure 8. (a) $\mathcal{S}(z)$ from (16); (b) expansion coefficients: $10^3\,\alpha_T[C^{-1}]$, dashed line; $-0.5 \times 10^3\,\alpha_s$ $[0/00^{-1}]$, dotted line; $10^3\,(\alpha_T + \mathcal{S}\alpha_s)$ $[°C^{-1}]$, solid line. These quantities are computed from θ and S profiles smoothed with 400 applications of Eqs. (1) and (2a) to the profiles of Figure 3 on a grid with $\Delta z = 10$ m.

right are not, except as residuals in this equation. We shall make an interpretation of these residuals below.

The combined expansion coefficient, $\alpha_T + \mathcal{S}\alpha_S$, and its components are plotted in Figure 8. Temperature effects are dominant throughout the profile, although salt contributions are not negligible. The resulting total mean advection,

$$A(z) = \mathbf{u} \cdot \nabla\theta + w\frac{\partial\theta}{\partial z}, \tag{25}$$

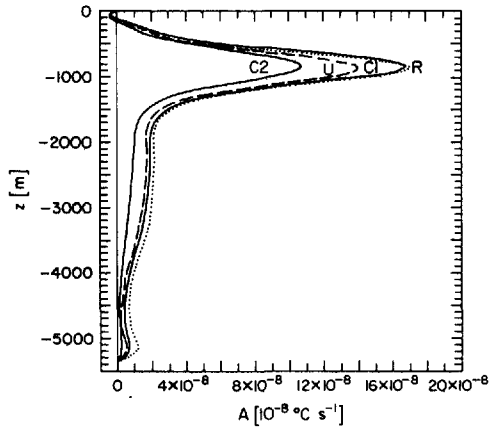

Figure 9. Mean advection of potential temperature from (25). 400 additional applications of the smoothing formulae (1) and (2) have been made to the profiles of Figures 3–4 and 6–7. The labeling convention is as in Figure 6.

the left side of Eq. (17), is plotted in Figure 9. The largest values are in the thermocline, and these imply a cooling tendency due to upwelling of colder water. This effect persists throughout most of the water column but is reversed near the upper surface, due to downward Ekman pumping. The predominance of positive advection values is due primarily to upward vertical advection, which itself has significant positive contributions from both w_s and the eddy flux term in (16). Even if the latter term were neglected (i.e., $r_0 = 0$), however, the net advection would still be mostly positive, as seen in Figure 5 by the predominance of $w_s > 0$. Only in the bottom km would there be some net warming (in profiles C1 and U). Mean horizontal advection vanishes in profiles C1 and C2, for the reason given following (24). For profiles R and U, it provides a warming tendency in the thermocline, with a magnitude roughly 20% of the cooling due to upwelling. Near the bottom, horizontal advection could also be important; profile R produces a cooling and U a warming.

As in the previous vorticity equation, the time derivative term has been neglected in (17). A scale estimate for this term can be constructed from an upper bound on the changes in θ in the deep water of 0.03°C (from comparing the different years' averages) and a lower bound on the time scale of 1 year. Thus

$$\left|\frac{\partial\theta}{\partial t}\right| < 0.1 \times 10^{-8}\text{°C}\, s^{-1}.$$

A comparison of this number with the mean advection profiles in Figure 9 shows that the neglect of $\partial\theta/\theta t$ is a reasonable approximation for most depths and profiles, although in a few circumstances (e.g., $z = -4800$ m and profile C2) the errors could be significant.

We shall interpret the residual from mean advection as eddy diffusion. Thus, we

formally make the following replacements for the flux divergencies in (17):

$$-\frac{\partial}{\partial z}(\overline{w'\theta'}) = \frac{\partial}{\partial z}\left(\kappa_v(z)\frac{\partial\theta}{\partial z}\right)$$
$$-\nabla\cdot(\overline{\mathbf{u}'\theta'}) = \nabla\cdot(\kappa_H(z)\nabla\theta). \tag{26}$$

If only the sum of vertical and horizontal diffusion is known, as is the case here, then the sum could be interpreted as either type. For such alternative interpretations, the ratio of the association diffusivities would be approximately

$$\frac{\kappa_v}{\kappa_H} \sim \mu^2,$$

where μ is the slope of the mean isothermal surface relative to horizontal, in order that the total diffusion be the same for each alternative.

By quasigeostrophic scaling arguments, mesoscale eddy processes should have a ratio of heat flux divergences implying

$$\frac{\kappa_v}{\kappa_H} \sim \left(\frac{R}{B}\right)^2\left(\frac{h}{l}\right)^2,$$

where R is a Rossby number ($=U/fl$) and B is a Burger number ($=N^2h^2/f^2l^2$) and h and l are characteristic vertical and horizontal scales of the general circulation [see, for example, Stone's (1972) analysis of the baroclinic instability problem]. If μ and (h/l) are approximately the same, then mesoscale eddies have a smaller ratio of diffusivities than the indistinguishable alternatives above since $R/B \ll 1$. We shall therefore adopt the following interpretation for the eddy diffusion alternatives: if mesoscale diffusion processes were dominant, κ_H would be the dominant diffusivity; whereas, if κ_v were dominant, the processes could not be mesoscale or else an excessively large κ_H would be indicated, and hence we would associate κ_v with submesoscale processes such as breaking internal waves.

First, we examine the possibility that the diffusion is wholly vertical; i.e., $\kappa_H = 0$. Then (17), (25), and (26) imply

$$\kappa_v(z) = \kappa_v(z_0) + \frac{1}{\partial\theta/\partial z}\int_{z_0}^{z} dz' A(z'), \tag{27}$$

We choose z_0 and the integration constant in (27) somewhat arbitrarily such that κ_v is a minimum at z_0 and its value there is 0.1 cm^2 s^{-1}; for each of the four velocity profiles in Figure 4, $z_0 = -H$. The result is shown in Figure 10 for the C1 velocity profile (results from other profiles are similar). The inferred values are quite large throughout most of the water column, and, as such, are insensitive to the small value chosen for $\kappa_v(z_0)$. These values are in fact too large by several orders of magnitude compared to direct

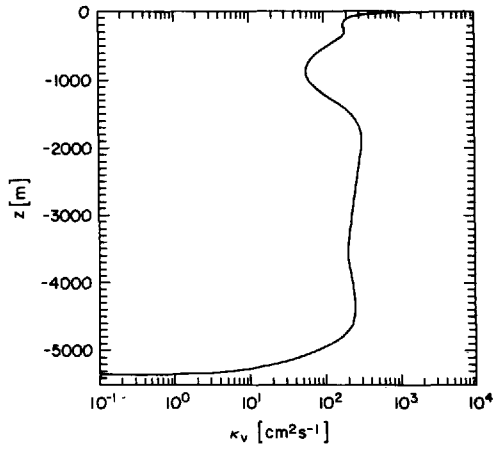

Figure 10. Vertical diffusivity for heat from (27), based upon velocity profile C1. Incremental smoothing is as in Figures 8 and 9.

estimates of κ_v in the ocean and the laboratory (Gregg and Sanford, 1980; Jenkins, 1980). Thus, we reject the hypothesis that the eddy diffusion is wholly vertical.

The extreme alternative is that the eddy diffusion is entirely horizontal ($\kappa_v = 0$). Hence, from (17) and (26),

$$\kappa_H(z) = \frac{\nabla\theta}{|\nabla\theta|^2} \cdot \int^x d\mathbf{x}' A. \tag{28}$$

We cannot evaluate (28) because it requires knowledge we do not have about the horizontal variation of $A(z)$. We are, therefore, forced to approximate (28) as

$$\begin{aligned} \kappa_H(z) &\approx L \frac{|A(z)|}{|\nabla\theta(z)|} \\ &= \frac{Lg(\alpha_T + \mathcal{S}\alpha_S)}{f\,|\partial\mathbf{u}/\partial z|} \left| \mathbf{u}\cdot\nabla\theta + w\frac{\partial\theta}{\partial z} \right| . \end{aligned} \tag{29}$$

In this final approximation, any depth dependence in the horizontal integral of (28) is lost, as is the directional information in the vector dot product.

The κ_H profiles from (29) are plotted in Figure 11 for $L = 200$ km, as before. A change in L would simply shift the abscissa in Figure 11. Also plotted are several more directly estimated diffusivities. Bryden (1982; Tables 1 and 3) lists thermocline values for both the numerator and denominator of

$$\kappa = -\,\overline{\mathbf{u}'T'} \cdot \nabla\overline{T} / |\nabla\overline{T}|^2,$$

based upon moored measurements; ∇T is calculated from $\mathbf{u}_z$, as in (23). For two types of averages, essentially the same two as for the mean velocities in Figure 4, one obtains

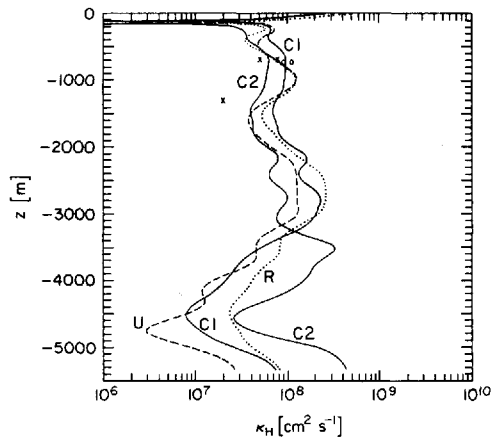

Figure 11. Horizonal diffusivity for heat from (29), based upon the four velocity profiles of Figures 4 and 7, with incremental smoothing as in Figures 8 and 9. Data points are directly measured diffusivities (0 = heat, x = particles) as described in the text.

values of 0.9 and 1.1 $\times$ 10^8 cm^2 s^{-1} for κ; these are the circles in Figure 11. Price (1983) has calculated single particle Taylor diffusivities from the rate of spreading of clusters of SOFAR floats. Zonal and meridonial diffusivities ($\kappa^{(x)}$, $\kappa^{(y)}$) at 700 m and 1300 m depths are respectively (0.8, 0.5) and (0.2, 0.2) $\times$ 10^8 cm^2 s^{-1}. These are plotted as crosses in Figure 10. There is, of course, no necessity for particles to be dispersed as heat is in situations where temperature is not dynamically passive; however, the two types of dispersion have been found to be similar in some relevant modeling studies (McWilliams and Chow, 1981), and we see that this is true for the LDE as well.

There is some indication that the particle diffusivities are slightly smaller than the thermal ones, but this feature is uncertain within the estimation errors quoted by the authors of the direct estimates. In any event, there is agreement to within half an order of magnitude between the inferred $\kappa_H(z)$ from (29) and the more directly estimated κ, $\kappa^{(x)}$, and $\kappa^{(y)}$ in the depth range where comparisons can be made. The worst agreement is with the 1300 m particle diffusivities, which are small relative to κ_H (1300 m). However, the former were estimated from a data set taken during a period dominated by Rossby wave motion (Price and Rossby, 1982), and are thus likely to underestimate the true mean diffusivity, which would also include contributions from other periods where the flow would be more turbulent and less wavelike.

This general agreement with directly estimated diffusivities gives credibility to the inferred values, which have the advantage of spanning the full depth of the ocean. Taking a broad view of the curves in Figure 11, averaging over different profiles and small vertical scale structures [including the leftward cusps associated with the near-surface zero in $A(z)$], we can conclude the following: $\kappa_H(z)$ is large, of order 10^8

$cm^2\,s^{-1}$, and nearly uniform over a broad depth range from near the surface to perhaps $z = -4000$ m. At greater depths the inference is more uncertain because of a sensitivity to uncertainties in the near-bottom velocity profile, but κ_H may be as large there as it is shallower.

Thus, on statistical grounds we cannot reject the hypothesis that the eddy heat diffusion is entirely horizontal. Of course, on physical grounds we would expect lesser, but non-zero vertical diffusion from both sub-mesoscale and mesoscale processes. We therefore conclude that thermal equilibrium in the Recirculation Zone is accomplished in the mean as a balance primarily between mean advection, mostly vertical, and mostly horizontal flux divergences associated with mesoscale eddies. These eddy heat fluxes are down-gradient ones, across mean isothermal surfaces, effecting a net warming in the Recirculation Zone by a diffusion of heat outwards from the warm core of the Gulf Stream Gyre.

The down-gradient characterization is correct at most depths since A is positive and the horizontal temperature gradient is in one quadrant (NW) because both velocity shear components are negative. Even near the surface, where $A < 0$, a down-gradient relation is possible if the temperature gradient reverses in sign as well. This is true at least at the surface where $\partial\theta/\partial y < 0$ (Oceanographic Atlas of the North Atlantic Ocean, 1967). We cannot assess accurately the sign of the mean temperature gradient in this depth interval from LDE measurements since there are too few available velocity measurements above 250 m depth.

5. Salt and density

The mean balance equations for both salt and density have the same forms as that for heat, (17), with mean advection balancing eddy flux divergences. Furthermore, from (19) and (20), small variations in both quantities are linearly proportional to $\delta\theta$, with the proportionality constant only a moderately variable function of depth (n.b., Fig. 8). Therefore, when arguments analogous to those of Section 4 are made for S or ρ, the inferred $\kappa_v(z)$ will be similar to Figure 10, the $\kappa_H(z)$ will be identical to Figure 11, and the summary conclusion about a balance primarily between mean advection and mesoscale horizontal diffusion will be the same.

6. Potential vorticity

Mean potential vorticity variations δq are defined as

$$\delta q = \beta\delta y - \frac{fg}{\rho_0}\frac{\partial}{\partial z}\left(\frac{\delta\rho}{N^2}\right) + \delta\zeta \tag{30}$$

under quasigeostrophic assumptions. Thus, with (18), we write the mean horizontal

gradients as

$$\frac{\partial q}{\partial x} = f^2 \frac{\partial}{\partial z}\left(N^{-2}\frac{\partial v}{\partial z}\right)$$
$$\frac{\partial q}{\partial y} = \beta - f^2 \frac{\partial}{\partial z}\left(N^{-2}\frac{\partial u}{\partial z}\right), \tag{31}$$

where $\nabla\zeta$ is neglected, as in Section 3 [n.b., a scale estimate of its relative magnitude is the same as the ratio preceding Eq. (9)]. The magnitude of ∇q can be interpreted as a wave propagation strength, where, crudely, a phase speed is $|\nabla q| \cdot k^{-2}$, with k a horizontal wavenumber. The sign reversal of ∇q with a depth is a necessary condition for baroclinic instability (Pedlosky, 1979). We see in Figure 12 that the propagation tendency exceeds the Rossby wave measure (i.e., $\beta = 2 \times 10^{-13}$ cm^{-1} s^{-1}) in both components of ∇q in some depth ranges. There are also multiple zero crossings, assuring that the necessary condition for instability is satisfied; Bryden (1982) and the discussion in Section 4 have shown that there are down-gradient eddy heat fluxes in the thermocline, which is a property associated with baroclinic instability. The vertical structure of $\nabla q(z)$ is complicated, but qualitatively similar for the different velocity profiles considered. The largest amplitudes occur near the bottom. This is because $N^{-2}(z)$ is much larger at depth, even though velocity shears are somewhat smaller there than in the thermocline.

There have been recent predictions of potential vorticity homogenization from theory and modeling (Holland, 1983; McWilliams and Chow, 1981; Rhines and Young, 1982): ∇q and $\overline{q'^2}$ should be very small in the ocean interior if sub-mesoscale, nonconservative processes are sufficiently weak (i.e., their eddy diffusivities are sufficiently small). Furthermore, there is empirical evidence from the historical archive of hydrographic data that mean potential vorticity does not have large horizontal variations between perhaps 250 m and 850 m depth in the North Atlantic Subtropical Gyre, which contains the Recirculation Zone (McDowell *et al.*, 1983). This feature is not obvious in our estimates of ∇q (Fig. 12), which are not particularly small in this depth interval.

The data presented in McDowell *et al.* (1983) are estimates of

$$Q = -\frac{f}{\rho_0}\frac{\partial \rho_\theta}{\partial z} = \frac{f}{g}N^2, \tag{32}$$

where ρ_θ is potential density. This is a definition of potential vorticity based upon somewhat different assumptions than (30): δQ and δq are not equivalent, although they have the same dynamical implications if we make the quasigeostrophic approximation and further neglect relative vorticity. We can compare our local estimate of Q with their data: it is simply f/g ($= 7.4 \times 10^{-8}$ s cm^{-1}) times $N^2(z)$, as plotted in Figure 3d. The resulting profile matches well their nearest data at (31N, 65W), with small differences attributable to the degree of smoothing. Thus, the small range of horizontal

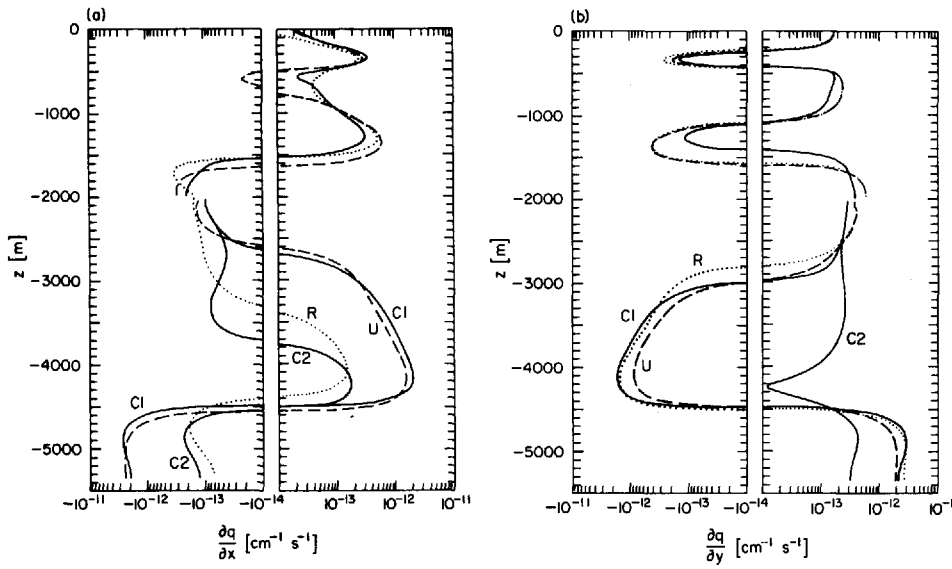

Figure 12. Mean potential vorticity gradients from (31). Incremental smoothing of **u** and N^2, starting from the profiles of Figures 3d and 4, has been performed by NS applications of (1)–(2). Above $z = -2000$ m, $NS = 400$, and below that level, $NS = 2000$.

variation of Q within the Subtropical Gyre, between the N^2 minimum in the 18°C thermostad and the N^2 maximum in the main thermocline, is confirmed in the LDE data.

However, what is dynamically important is not the size of the absolute variations of Q; rather it is the size of the relative variations at a fixed depth (or on a fixed potential density surface—the quasigeostrophic approximation does not make a significant distinction between the two in this regard). This aspect of the Q distribution is best demonstrated in their Figures 17–19, which are plots against latitude of Q averaged within three adjacent layers defined by particular surfaces of constant potential density. In each plot data are included from two sections (50W and 65W) which pass through the Recirculation Zone, as drawn in Figure 1a, and for comparison the contribution to Q variations from β is also plotted. These Q plots are adapted slightly as our Figure 13. The scatter in these plots is considerable, which makes interpretation difficult. However, our own estimates of ∇q from (31) are also of questionable accuracy since the indicated vertical scale is not large and a second vertical derivative of velocity is a difficult calculation to make from moderately uncertain mean velocity measurements. Nevertheless, a comparison of the two types of estimates indicates substantial agreement.

The shallowest of the three layers contains the N^2 minimum, and occurs between 200 and 400 m depth at the LDE site. The Q data show a northward decrease, opposite to the β-effect, until the approximate location of the Gulf Stream. In addition, the Q

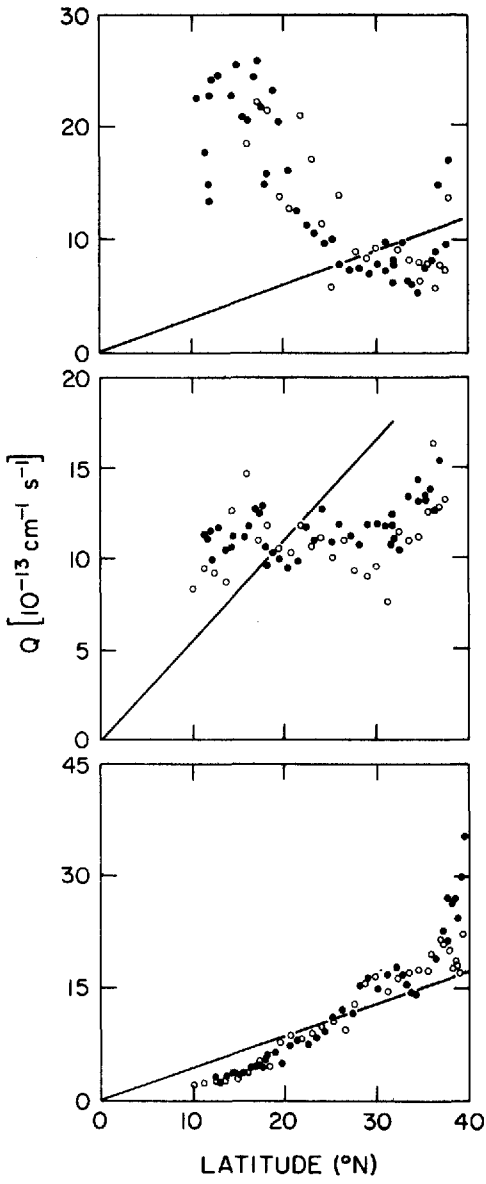

Figure 13. Potential vorticity from (32), as calculated by McDowell *et al.* (1983), from which this figure was adapted. The data points are coded by longitude: closed circles are from 65W and open circles are from 50W. The plots are for layers bounded by surfaces of constant ρ_θ: the upper has bounds [1.0263, 1.0265], the middle [1.0265, 1.0270], and the lower [1.0270, 1.0273]. The lines indicate the contributions to Q variations from β alone.

values along 50W appear to be somewhat larger than those along 65W in the Recirculation Zone. No substantial region of homogenization is indicated. The local estimates in Figure 12 show

$$\frac{\partial q}{\partial y} < 0, \qquad \frac{\partial q}{\partial x} > 0$$

in this depth interval, with comparable magnitudes for each component, which is wholly consistent with the Q variations.

The middle layer extends from just below the N^2 minimum to just above the N^2 maximum, 400–700 m depth at the LDE site. The Q data show a very extensive region north of about 15N where any large-scale variations are substantially less than the β-effect, and significant homogenization could be occurring. However, the northern edge of this region appears to coincide with the southern edge of the Recirculation Zone, near 30N. Northward of this point, Q increases at approximately the rate due to β. The Q values appear to be somewhat smaller along 50W than along 65W, although this difference, if real, is smaller relative to the β-effect than the zonal difference in the upper layer. Again the comparison with our local estimates is very good. $\partial q/\partial y$ is positive with about the value of β, indicating that the homogeneous region, if it exists in this layer, does not extend into the Recirculation Zone. $\partial q/\partial x$ is locally diminished in this layer, and perhaps negative (profile U). The zonal gradient of mean potential velocity does appear to be small in the upper thermocline of the Recirculation Zone.

The lowest of the three layers contains the N^2 maximum, 700–850 m depth locally. The Q data show a northward increase at about the rate due to β and a narrow region of eastward increase in the center of the Recirculation Zone, which decreases to a small, uncertain zonal trend on the southern edge. This is again in good agreement with the estimates in Figure 12: $\partial q/\partial y \approx \beta$, and $\partial q/\partial x$ is more weakly positive.

In summary, therefore, the qualitative features of our local ∇q estimates are confirmed in the large-scale analysis of McDowell *et al.* (1983), and one can at least tentatively reject the occurrence of homogenization, at any level significantly below the contributions from β, in and above the thermocline in the Recirculation Zone. The theoretical predictions of homogenization assume vanishingly small values for sub-mesoscale eddy flux divergences. Perhaps homogenization does not occur in the ocean because these processes are not sufficiently weak. In support of this possibility, Brown and Owens (1981) have estimated a sub-mesoscale horizontal diffusivity for momentum of 3×10^6 cm^2 s^{-1} in the thermocline in the LDE, and, above the thermocline in the 18°C thermostad, wintertime boundary layer turbulence is strong. It is unclear whether these are sufficient to obviate the $\nabla q \approx 0$ prediction in principle.

The mean balance equation for potential vorticity is

$$\mathbf{u} \cdot \nabla q = - \nabla \cdot (\overline{\mathbf{u}' q'}), \tag{33}$$

again with a small Rossby number assumption. This is a reformulation of the vorticity

equation (7), where the eddy fluxes of both relative and stretching vorticity explicitly enter on the right side [see (35) below]. From (31),

$$\mathbf{u}\cdot\nabla q = \beta v + f^2\left[u\frac{\partial}{\partial z}\left(N^{-2}\frac{\partial v}{\partial z}\right) - v\frac{\partial}{\partial z}\left(N^{-2}\frac{\partial u}{\partial z}\right)\right]. \tag{34}$$

Another aspect of the homogenization prediction discussed above is that the potential enstrophy $\overline{q'^2}$ should vanish. From (33), we see that this cannot happen unless the mean q advection vanishes (i.e., $\overline{q'^2}$ cannot vanish over a region while $\nabla\cdot\overline{\mathbf{u}'q'}$ is required to remain nonzero). This mean advection is plotted in Figure 14. In profiles C1 and C2, $u \equiv v$, and the advection is simply βv. In these profiles there is thus no indication of vanishing advection at other than a single depth. Profiles R and U show more complexity with depth, and, relevant to the prediction, they indicate a locally diminished advection in the 18°C thermostad. The true character of this feature is, unfortunately, hidden by the large uncertainties in our estimates, as indicated by the variations among the profiles. These uncertainties are so large below the thermocline as to make any interpretation doubtful.

The mean q balance in (33) and (34) is implicit in previous inferences of vorticity and heat balances. The eddy flux divergence can be decomposed as follows:

$$-\nabla\cdot(\overline{\mathbf{u}'q'}) = -\nabla\cdot(\overline{\mathbf{u}'\zeta'}) - \nabla\cdot(\overline{\mathbf{u}'\chi'}), \tag{35}$$

where

$$\chi' = -\frac{fg}{\rho_0}\frac{\partial}{\partial z}\left(\frac{\rho'}{N^2}\right) \tag{36}$$

is the eddy stretching vorticity [analogous to the second term in (30)]. By the arguments of Section 3, we estimate the relative vorticity flux divergence as

$$-\nabla\cdot(\overline{\mathbf{u}'\zeta'}) = r_0, \tag{37}$$

where values for r_0 are listed in Table 1. By previously presented arguments, we can also derive the following relations:

$$\begin{aligned}
-\nabla\cdot(\overline{\mathbf{u}'\chi'}) &= \frac{fg}{\rho_0}\frac{\partial}{\partial z}\left(\frac{1}{N^2}\nabla\cdot(\overline{\rho'\mathbf{u}'})\right)\\
&= -f\frac{\partial}{\partial z}\left(\frac{1}{\partial\theta/\partial z}\nabla\cdot(\overline{\mathbf{u}'\theta'})\right)\\
&= f\frac{\partial}{\partial z}\left[w + (\mathbf{u}\cdot\nabla\theta)\Big/\frac{\partial\theta}{\partial z}\right]\\
&= -r_0 + f\frac{\partial}{\partial z}\left[w_s + (\mathbf{u}\cdot\nabla\theta)\Big/\frac{\partial\theta}{\partial z}\right]\\
&= -r_0 + \mathbf{u}\cdot\nabla q.
\end{aligned} \tag{38}$$

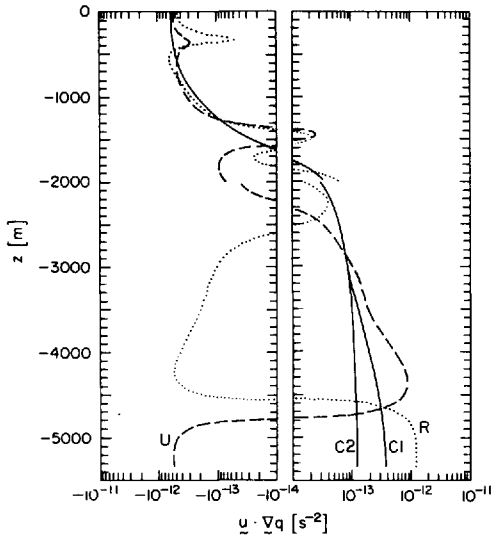

Figure 14. Mean potential vorticity advection from (34) and the profiles of Figure 12.

The final relation in (38), of course, makes (33) an identity when combined with (35) and (37). The penultimate relation in (38) shows that the stretching vorticity flux divergence opposes the relative vorticity flux and contributes an additional term as well (which is equal to what is plotted in Fig. 14). This additional term is related to the mean heat advection without the enhanced vertical advection driven by r, and its balancing eddy heat flux is also predominantly down-gradient because $w_s \cdot \partial\theta/\partial z$ is predominantly positive (n.b., the discussion following (25) in Section 4). Brown and Owens (personal communication) have calculated the fluxes in (35) at 700 m depth from LDE moored measurements, although their divergences could not be calculated. They found, firstly, that $\overline{\mathbf{u}'\chi'}$ was nearly an order of magnitude larger than $\overline{\mathbf{u}'\zeta'}$ and, secondly, that $\overline{\mathbf{u}'q'}$ had a magnitude of 2×10^{-5} cm s^{-2} directed toward 210° true. The ∇q at 700 m from Figure 12 has a magnitude of about 2×10^{-13} cm^{-1} s^{-1} directed toward NNW. Thus, a potential vorticity diffusivity is 1×10^{8} cm^2 s^{-1}, acting almost directly downgradient.

The stretching vorticity flux is thus dominant and is associated with the down-gradient (i.e., positive diffusivity) heat flux described in Section 4. This suggests that the subordinate relative vorticity flux, acting in opposition, is a counter-gradient (i.e., negative horizontal eddy viscosity) process. This was also suggested from the signs of r and ζ in Section 3. Unfortunately, not enough is known of the spatial structure of the general circulation to confirm the suggestion. In some modeling studies (e.g., McWilliams and Chow, 1981), these relations between the different fluxes have been demonstrated.

The ∇q profiles in Figure 12, while not "homogeneous," do provide nontrivial

constraints upon eddy potential vorticity q'. If a fluid parcel initially at rest traverses a horizontal distance while conserving $q + q'$, then

$$q' = - \triangle \mathbf{x} \cdot \nabla q. \tag{39}$$

Sufficiently intense, locally generated (i.e., $| \triangle \mathbf{x} | < L$) eddy motions, if they occur, will have ζ' and χ' magnitudes much larger than q'. Consistency thus requires a degree of negative correlation between ζ' and χ', at a level set by (39) and the eddy intensity. Hua and Owens (1983) have demonstrated that this correlation exists in the LDE thermocline. This negative correlation also gives further support to the idea that the stretching and relative vorticity flux divergences in (35) are acting in opposition.

7. Energy and momentum

In this section, some remarks are made about two mean dynamical balances which cannot be fully described from present observations.

A complete characterization of the mean energy balance is not feasible, because of unknown lateral fluxes, bottom boundary layer dissipation, and pressure work. However, Bryden (1982) has made estimates of some terms in the balance, the local rates of mean energy loss or gain in the LDE thermocline through interactions with mesoscale eddies. He has found that the loss of mean potential energy to the eddies through baroclinic conversion processes (e.g., baroclinic instability) is significant, while the loss or gain of mean kinetic energy due to correlations between the divergences of horizontal eddy Reynolds stresses and mean velocities is at least an order of magnitude smaller. On the other hand, the loss of eddy kinetic energy through correlations between horizontal Reynolds stresses and mean horizontal shear is positive, although smaller in magnitude than the baroclinic conversion process. Unfortunately, this estimate has substantial uncertainties due to its dependence upon $\nabla \mathbf{u}$ (n.b., Section 2c). The imbalance between the two types of kinetic energy conversion, if real, would suggest the importance of lateral energy fluxes in the Recirculation Zone.

The baroclinic loss from the mean is consistent with down-gradient heat flux (Section 4) and stretching vorticity flux dominance (Section 6). From a counter-gradient momentum flux (Sections 3 and 6), one would expect a transfer of kinetic energy from the eddies to the mean at least in a volume average, whereas the preceeding evidence is ambiguous.

If there is a prevalent counter-gradient momentum flux in the Recirculation Zone, then it would provide a force driving the northeastward Reverse Flow below the thermocline, insofar as momentum is being transferred horizontally, with negative viscosity, from a hypothetical deep, southwestward Return Flow nearer to the Gulf Stream. Another force is associated with the down-gradient heat fluxes; it is often called isopycnal form drag, and it is characterized by a positive vertical eddy viscosity (McWilliams and Chow, 1981). Such a process would provide a local retarding force

for the Reverse Flow, since this lies beneath an opposite Return Flow in the thermocline.

However, form drag may be a significant cause of the deep Reverse Flow, through action from a distance. In an analysis of the Deep Counter-rotating Gyre (see Fig. 5) in a numerical model solution, Holland and Rhines (1980) showed that form drag was the primary source of momentum for the gyre as a whole. Its accelerating effects, though, would occur in the northern branch, where Return Flow occurs in both the thermocline and deeper, and form drag can transfer westward momentum downward. One can therefore imagine that the southern Reverse Flow branch exists primarily to close the gyre mass budget for the more strongly driven deep Return Flow in the north. In this case, the local driving force in the Reverse Flow would be a weak, westward pressure gradient.

These two possibilities for Return Flow driving forces are not mutually exclusive; either or both may be occurring.

8. Summary and discussion

In this paper, an analysis has been made of the estimated mean hydrographic and horizontal velocity profiles in the southern part of the Recirculation Zone. The flow in and above the thermocline is to the southwest and is presumably part of the Return Flow for the Gulf Stream Gyre. Below the thermocline the flow is to the northeast, which is referred to as a deep Reverse Flow. In an analysis of the mean vorticity balance, an inference is made of a generally upward mean vertical velocity, balanced partly by a nearly depth-independent eddy relative vorticity flux divergence. These inferences follow from calculations of the planetary vorticity advection, which implies a mid-depth maximum in the Sverdrup velocity, and of the top (Ekman) and bottom (topographic) boundary conditions. The latter in particular implies a large upward w due to a horizontal velocity across topographic contour lines. In an analysis of the mean heat balance, an inference is made of a significant horizontal eddy heat flux acting in opposition to a net cooling by mean advection through most of the water column. This heat flux can be characterized by a positive lateral eddy diffusivity on the order of 10^8 $cm^2\,s^{-1}$. Mean potential vorticity gradients exhibit moderately strong, though complex, possibilities for wave propagation and baroclinic instability. They do not, however, show a region of homogenization. In the mean potential vorticity balance, the eddy flux divergence balances the mean advection, with stretching vorticity dominating relative vorticity in the flux. The two types of vorticity flux divergence provide opposing tendencies in the potential vorticity balance.

Many of the previous diagnoses of the general circulation have been concerned with inferring the horizontal velocity from the three-dimensional structure of density (this, of course, is not our present concern because velocity measurements are available from the LDE). The methods of Stommel and Schott (1977), Davis (1978), and Wunsch (1978) all assume conservation in the mean of density and/or potential vorticity. As we

have seen in Sections 4–6, this appears to be incorrect for both quantities in the Recirculation Zone: the eddy flux divergences are not negligible in the mean balance equations. Thus, such methods are probably inapplicable in this region and others where mesoscale eddy energies, and presumably fluxes, are large. A similar conclusion was reached by Keffer and Niiler (1982) for other sites in the North Atlantic with even less mesoscale energy than the Recirculation Zone.

It is worth remarking that the inferrential method of this paper requires measurements from only a single mooring, assuming that sufficient hydrographic data are available to estimate mean profiles. We have made some use of measurements from multiple moorings (e.g., for estimating $\overline{\mathbf{u}'\zeta'}$ and ζ), but only to check the consistency of the single mooring inferences. The justification for this comes from sampling error considerations. In the LDE, the estimated vertical shear in $\mathbf{u}$ across the thermocline is clearly significant, while the horizontal shear is not (see Section 2c). It also seems preferable to base the inferences upon directly measured $\mathbf{u}(z)$ time series from moorings rather than $\nabla\rho(z)$ from shipboard hydrographic profiles, even though in theory their information content is largely redundant [n.b., Eq. (18)], simply because it is difficult to obtain enough independent samples of the latter where eddy variability is substantial. For estimates of very large-scale currents rather than local ones, however, the sampling advantage shifts to $\nabla\rho$ if somehow a large-scale reference level can be determined.

In any of the present diagnostic models, however, sampling errors are significant contaminants of the inferences. Ours is no exception. Within the measurement uncertainties for horizontal velocity (Section 2), the true mean profiles could be such that mean advections of heat, salt, density, and potential velocity could be zero in any small depth interval, so that our inferences of significant mesoscale eddy flux divergences could be nullified. Also, the mean potential vorticity gradients could be made zero locally. To do this, however, would require deforming the velocity profiles away from the estimated point means, as well as introducing unsubstantiated, small-scale vertical structure in the profiles. This would not be a straightforward or unprejudiced data analysis, though, nor would its result be consistent with the available point measurements of eddy fluxes (e.g., the data points in Fig. 11). Hence, we judge our inferences more plausible than the alternatives above, but they are far from being deductions.

Acknowledgments. Helpful discussions during the course of this work were held with Harry Bryden, Roland deSzoeke, William Holland, Lien Hua, Tom Keffer, Brechner Owens, Peter Niiler, Peter Rhines, and Bruce Taft. Computations were made by Julianna Chow and Nancy Norton. Financial sponsorship was by the National Science Foundation at the National Center for Atmospheric Research.

REFERENCES

Bradley, A., C. Ebbesmeyer, J. McWilliams, T. Rossby and B. Taft. 1977. Preliminary report for POLYMODE Cruise: R/V *Endeavor* 7. POLYMODE News, 29, Woods Hole Oceanographic Institution.

Brown, E. D. and W. B. Owens. 1981. Observations of the horizontal interactions between the internal wave field and the mesoscale flow. J Phys Oceanogr., *11,* 1474–1480.

Bryden, H. L. 1973. New polynomials for thermal expansion, adiabatic temperature gradient, and potential temperature of sea water. Deep-Sea Res., *20,* 401–408.

—— 1976. Horizontal advection of temperature for low-frequency motions. Deep-Sea Res., *23,* 1165–1174.

—— 1982. Sources of eddy energy in the Gulf Stream recirculation region. J. Mar. Res., *40,* 1047–1068.

Bryden, H. and R. Millard. 1980. Spatially averaged Local Dynamics Experiment CTD stations. POLYMODE News, 77, Woods Hole Oceanographic Institution.

Davis, R. E. 1978. On estimating velocity from hydrographic data. J. Geophys. Res., *83,* 5507–5509.

Ebbesmeyer, C., B. A. Taft, J. C. McWilliams, C. Y. Shen, S. C. Riser, H. T. Rossby, P. E. Biscaye and H. G. Ostlund. 1983. Variability of physical and chemical properties along a Northwestern Atlantic Oceanographic Section (23–33N: 70W), J. Phys. Oceanogr., (submitted).

Fofonoff, N. P. 1963. Precision of oceanographic data for sound speed calculations. J. Acous. Soc. Am., *35,* 830–836.

Gregg, M. C. and T. B. Sanford. 1980. Signatures of mixing from the Bermuda Slope, the Sargasso Sea and the Gulf Stream. J Phys. Oceanogr., *10,* 105–127.

Holland, W. R. 1978. The role of mesoscale eddies in the general circulation of the ocean: Numerical experiments using a wind-driven quasi-geostrophic model. J. Phys. Oceanogr., *8,* 363–392.

—— 1983. Well-mixed regions of potential vorticity in numerical models of midlatitude ocean circulation, (in preparation).

Holland, W. R. and P. B. Rhines. 1980. An example of eddy-induced ocean circulation. J. Phys. Oceanogr., *10,* 1010–1031.

Hua, B.-L. and W. B. Owens. 1983. Estimates of eddy potential vorticity and its balance in the POLYMODE Local Dynamics Experiment, (in preparation).

Jenkins, W. S. 1980. Tritium and ^{3}He in the Sargasso Sea. J. Mar. Res., *38,* 533–569.

Keffer, T. and P. P. Niiler. 1982. Eddy convergence of heat, salt, density, and vorticity in the sub-tropical North Atlantic. Deep-Sea Res., *29,* 201–216.

Leetmaa, A. and A. F. Bunker. 1978. Updated charts of the mean annual wind stress, convergences in the Ekman layers, and Sverdrup transports in the North Atlantic. J. Mar. Res., *36,* 311–322.

Lindstrom, E. J., D. W. Behringer, B. A. Taft and C. C. Ebbesmeyer. 1980. Absolute velocity determination from historical hydrographic data in the western North Atlantic. J. Phys. Oceanogr., *10,* 999–1009.

Mantyla, A. W. 1980. Electrical conductivity comparisons of standard seawater batches P29 to P84. Deep-Sea Res., *27,* 837–846.

McDowell, S., P. Rhines and T. Keffer. 1983. North Atlantic potential vorticity and its relation to the general circulation. J. Phys. Oceanogr., *12,* 1417–1436.

McWilliams, J. C. and J. H. S. Chow. 1981. Equilibrium geostrophic turbulence: a reference solution in a β-plane channel. J. Phys. Oceanogr., *11,* 921–949.

McWilliams, J. C. *et al.* (21 authors). 1982. The local dynamics of eddies in the western North Atlantic. Eddies in Mar. Sci., A. R. Robinson, ed., (in press).

Oceanographic Atlas of the North Atlantic Ocean. Section II Physical Properties, 1967, U.S. Naval Oceanographic Office, Pub. No. 700, Washington, DC, 300 pp.

Owens, W. B. 1983. Empirical, orthogonal modes for the POLYMODE Local Dynamics Experiment, *(in preparation).*

Owens, W. B., J. R. Luyten and H. L. Bryden. 1982. Moored velocity measurements on the edge of the Gulf Stream recirculation. J. Mar. Res., *40,* (Suppl.), 509–524.

Pedlosky, J. 1979. Geophysical Fluid Dynamics. Springer-Verlag, New York, 624 pp.

Pillsbury, R. D., J. Bottero, R. E. Still and E. P. Laine. 1982. Data Report for Current Meters on Mooring CMME-1, 1980–81; Atlantic Study Area E-N3, Report OSU-15, School of Oceanography, Oregon State University, Corvallis, Oregon.

Pratt, R. M. 1968. Atlantic continental shelf and slope of the United States—physiographic and sediments of the deep-sea basin. Geo. Sur. Prof. Paper 529-B, U.S. Government Printing Office, Plate I.

Price, J. F. 1983. Particle dispersion in the western North Atlantic. J. Geophys. Res., (submitted).

Price, J. and H. T. Rossby. 1982. Observations of a planetary wave during the Local Dynamics Experiment. J. Mar. Res., *40,* (Suppl.), 543–558.

Rhines, P. B. and W. Young. 1982. Homogenization of potential vorticity in planetary gyres. J. Fluid Mech., *122,* 347–368.

Schmitz, W. J., Jr. 1977. On the deep general circulation in the western North Atlantic. J. Mar. Res., *35,* 21–28.

—— 1980. Weakly depth-dependent segments of the North Atlantic circulation. J. Mar. Res., *38,* 111–133.

Schmitz, W. J., Jr. and W. R. Holland. 1982. A preliminary comparison of selected numerical eddy-resolving general circulation experiments with observations. J. Mar. Res., *40,* 75–117.

Stommel, H. and F. Schott. 1977. The beta-spiral and the determination of the absolute velocity field from hydrographic station data. Deep-Sea Res., *24,* 325–329.

Stone, P. H. 1972. On non-geostrophic baroclinic instability: Part III. The momentum and heat transports. J. Atmos. Sci., *29,* 419–426.

Taft, B. A., C. C. Ebbesmeyer, E. J. Lindstrom, J. C. McWilliams and C. Y. Shen. 1983. Hydrographic property variability from the POLYMODE Local Dynamics Experiment, J. Phys. Oceanogr., (submitted).

Tarbell, S. and A. Spencer. 1978. A compilation of moored current data and associated observations. Woods Hole Oceanographic Institution Technical Report 78-5, Woods Hole, Massachusetts.

TTO. 1981. North Atlantic Study, Preliminary Leg Reports, PACODF, Scripps Institution of Oceanography.

Uchupi, E. 1971. Bathymetric Atlas of the Atlantic, Caribbean, and Gulf of Mexico. Woods Hole Oceanographic Institution Technical Report, WHOI, 71–72.

Worthington, L. V. 1976. On the North Atlantic Circulation. Johns Hopkins Oceanographic Studies, *6,* 110 pp.

Worthington, L. V. and W. R. Wright. 1970. North Atlantic Ocean Atlas of Potential Temperature and Salinity in the Deep Water. Woods Hole Oceanographic Institution, The Woods Hole Oceanographic Institution Atlas Series, Vol. II.

Wunsch, C. 1978. The general circulation of the North Atlantic west of 50W determined from inverse methods. Rev. Geophys. Space Phys., *16,* 583–620.

Received: *30 July, 1982;* revised: *25 January, 1983.*